Analysis of the reflective-matched fiber Bragg grating sensing interrogation scheme

A. B. Lobo Ribeiro, L. A. Ferreira, J. L. Santos, and D. A. Jackson

A technique for the demodulation of fiber Bragg grating (FBG) sensors based on the use of a second wavelength-matched FBG receiver to track wavelength shifts from the FBG sensor is analyzed, particularly regarding its sensitivity as determined by primary noise sources. Numerical and experimental results show that there is an optimum Bragg wavelength difference between the two FBG's that maximizes the sensitivity for this demodulation technique. © 1997 Optical Society of America

Key words: Fiber Bragg gratings, optical fiber sensors, strain sensors.

1. Introduction

Fiber Bragg gratings (FBG's) are attracting considerable interest for application as sensing elements,[1,2] because of their intrinsic nature and inherent wavelength-encoded operation. Encoding the information about the measurand in a wavelength form has several distinct advantages over direct intensity-based sensing schemes. The most important advantage is that wavelength is an absolute parameter and thus does not depend on losses in the system or fluctuations in the source power. This feature allows for a straightforward determination of the grating-induced strain or temperature by means of a simple measurement of the wavelength shift reflected by the sensing element. This shift can be determined with monochromators or optical spectrum analyzers, albeit quite slowly. However, its not feasible to use instruments of this type for practical applications because of their size and weight and the frequent need for recalibration. Thus, the cost of a FBG-based strain or temperature sensor system may be determined more by the demodulation unit than by the sensor head itself. Most demodulation techniques developed to date rely on optical filtering methods, such as bulk optical edge filters,[3] scanning fiber Fabry–Perot filters,[4] wavelength-division fiber couplers,[5,6] acousto-optic tunable filters,[7] and Mach–Zehnder interferometers.[8]

Recently, an approach to demodulate the wavelength shift from a FBG sensor, which also relies on optical filtering, has been proposed and demonstrated.[9,10] The basic principle of operation of this technique is the use of a wavelength-matched receiver FBG to filter the returned signal from a sensing FBG.[9] For this to be done, the two gratings are fabricated with nominally equal Bragg wavelengths, and the temperature or strain-induced shifts in the sensing FBG can be tracked by the receiving FBG by using a controllable strain element attached, such as a piezoelectric transducer. The receiving FBG can operate as a bandpass filter (reflective mode)[10] or as a reflective notch filter (transmissive mode). The principle of operation is identical but there is an improvement of sensor sensitivity in the transmissive mode that is due to a smaller power loss.[11]

In this paper the matched FBG demodulation technique is investigated. By consideration of primary noise sources, it is shown that there is an optimum wavelength tuning difference between the two FBG's that maximizes the sensitivity of this demodulation scheme for measurand recovery.

2. System Power Budget

The basic configuration of the sensor–receiver grating pair scheme[9] is shown in Fig. 1. Light from a broadband source (BBS) is transferred to the sensing grating (FBG_S) by means of a directional coupler with nominal coupling ratio (k), and the light reflected from the FBG_S then propagates back through the fiber network to the receiving grating (FBG_R), which will perform a matched filter function.

D. A. Jackson is with the Applied Optics Group, Physics Laboratory, University of Kent, Canterbury, Kent CT2 7NR, United Kingdom. The other authors are with the Grupo de Optoelectrónica, Instituto de Engenharia de Séstemas e Computadores, Rua José Falcão 110, 4000 Porto, Portugal. J. L. Santos is also with the Laboratório de Física, Universidade do Porto, Praça Gomes Teixeira, 4000 Porto, Portugal.

Received 20 February 1996.
0003-6935/97/040934-06$10.00/0

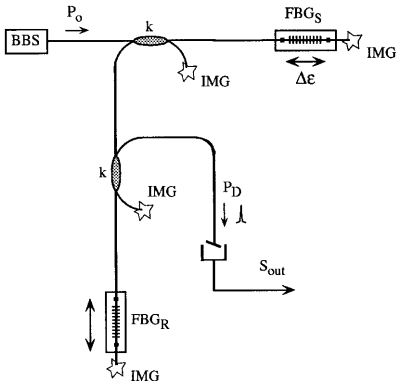

Fig. 1. Diagram of the sensor–receiver grating pair scheme; IMG, index matching gel.

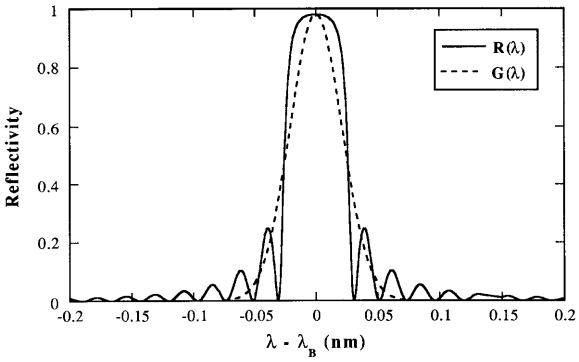

Fig. 2. Spectral dependence of the FBG reflectivity, considering the exact model, $R(\lambda)$, and the Gaussian approximation, $G(\lambda)$, for $\lambda_B = 830$ nm.

Considering a BBS, such as an edge-emitting LED or a superluminescent diode, with a smooth spectral profile, its spectrum can be modeled as a Gaussian distribution of wavelengths with a spectral full width at half-maximum (FWHM) of $\Delta\lambda_0$ and a center wavelength of λ_0. Hence the Gaussian model gives

$$S(\lambda) = I_{\text{peak}} \exp\left[-4 \ln 2\left(\frac{\lambda - \lambda_0}{\Delta\lambda_0}\right)^2\right], \tag{1}$$

where λ is the wavelength in vacuum and I_{peak} is the peak power. Here $I_{\text{peak}} = (P_0/\Delta\lambda_0)[(4 \ln 2/\pi)^{1/2}]$, where P_0 is the total power injected into the system by the BBS. However, for many real sources the profile is more complex than described by Eq. (1), as a fine periodic structure is often superimposed on the Gaussian profile. Depending on the modulation depth of this fine structure, the spectral profile of the light reflected from a FBG can be distorted, leading to a scale error factor in the measurement of the Bragg wavelength shift.[12] Thus it is necessary to ensure that the spectral profile of the source is smooth, and in our experiment the profile was found to be particularly flat in the working range of the FBG sensor.

To calculate the spectral response (i.e., the reflectivity) of a FBG, one can use the coupled mode theory. Assuming the grating has a refractive index modulation with constant amplitude (Δn_0) and period (Λ), the solution of the coupled mode equations for the forward- and backward-traveling waves in the fiber containing the grating shows that its reflectivity is given by[13]

$$R(\lambda) = \frac{|\Omega|^2 \sinh^2(sL)}{\Delta\beta^2 \sinh^2(sL) + s^2 \cosh^2(sL)}, \tag{2}$$

where $\Delta\beta = 2\pi n_{\text{eff}}[(1/\lambda) - (1/\lambda_B)]$ is the differential propagation constant associated with the detuning from the Bragg condition ($\lambda = \lambda_B = 2n_{\text{eff}}\Lambda$), n_{eff} is the average effective refractive index of the fiber grating, L is its length, Ω is the coupling coefficient, and $s = (|\Omega|^2 - \Delta\beta^2)^{1/2}$. For a uniform grating, Ω is a constant (generally a complex number) and is dependent on the induced refractive index perturbation along the fiber axis. For a sinusoidally modulated refractive index with the form[13,14]

$$n(z) = n_{\text{eff}} + \Delta n = n_{\text{eff}} + \Delta n_0 \cos\left(\frac{2\pi z}{\Lambda}\right), \tag{3}$$

Ω is real and is given by

$$\Omega = \frac{\pi \Delta n_0}{\lambda} \chi, \tag{4}$$

where Δn_0 is the refractive index modulation depth of the grating and χ is the fraction of the integrated fundamental mode intensity contained in the fiber core.[14] For a real grating the index modulation function, $n(z)$, is not necessarily sinusoidal even if the UV interference pattern used to write the grating is sinusoidal. This results from the nonlinear response of the fiber index change to the UV light intensity.[13] Because of this, $n(z)$ may deviate from a sinusoidal function, thereby originating a different reflectivity response.

The reflective dependence given by Eq. (2) is complex, as it is difficult to treat analytically. Considerable simplification is possible if it is assumed that the Bragg grating reflectivity function can be modeled as a Gaussian function with a center wavelength (or Bragg wavelength) of λ_B and spectral FWHM, $\Delta\lambda_B$, equal to the one associated with relation (2):

$$G(\lambda) = R_0 \exp\left[-4 \ln 2\left(\frac{\lambda - \lambda_B}{\Delta\lambda_B}\right)^2\right], \tag{5}$$

where R_0 is the maximum reflectivity that occurs at the Bragg wavelength. Figure 2 shows the two reflectivity distributions [Eqs. (2) and (5)] for the case in which $L \approx 10$ mm, $\Delta n_0 = 1.0 \times 10^{-4}$, $n_{\text{eff}} = 1.452$, $\chi = 0.7$, $\lambda_B = 830$ nm, and R_0 is equal to the maximum reflectivity in Eq. (2), which is given by $\tanh^2(\Omega L)$. It is clear from this figure that the Gaussian curve follows fairly well the average dependence shown by Eq. (2), but obviously it cannot reproduce its fine structure. Therefore, the Gaussian approximation has to be considered with care. However, it is shown below that in the context of the problem addressed in this paper, the Gaussian model works well.

As the spectral width of the BBS is much larger than the spectral width of the FBG, i.e., $\Delta\lambda_0 \gg \Delta\lambda_B$, it is valid to state that the spectral distribution of wavelengths reflected from the grating when illuminated by the BBS (not considering the losses through the fiber network) is given by

$$I_S(\lambda) = S(\lambda_B)G(\lambda), \tag{6}$$

where $S(\lambda_B)$ is given by Eq. (1) when $\lambda = \lambda_B$. The total power reflected by the FBG is the integral of Eq. (6) over all the wavelength range.

For the demodulation scheme analyzed here (Fig. 1), it is assumed that the FBG_S and the FBG_R have identical reflectivity dependencies given by Eq. (6); in what follows, indices S and R refer to the sensing and receiving gratings, respectively. The reflected light from the FBG_S after passing the second directional coupler will be filtered by the receiving grating. If now the Bragg wavelength of the FBG_R (λ_{BR}) is identical to the Bragg wavelength of the FBG_S (λ_{BS}), then a strong signal will be backreflected from the FBG_R and detected by the photodiode (see Fig. 1; in the transmissive configuration[11] no signal is detected in this situation). The analysis of the scheme shown in Fig. 1 indicates that the total optical power arriving at the photodetector is given by

$$P_D = k^2(1-k)^2 \int_{-\infty}^{+\infty} S(\lambda_{BS})G_S(\lambda)G_R(\lambda)\mathrm{d}\lambda, \tag{7}$$

or

$$P_D = k^2(1-k)^2 S(\lambda_{BS}) \frac{R_{0R}R_{0S}\sqrt{\pi}}{\sqrt{4\ln 2}} \times \left\{ \frac{\Delta\lambda_{BS}\Delta\lambda_{BR}}{(\Delta\lambda_{BS}^2 + \Delta\lambda_{BR}^2)^{1/2}} \times \exp\left[-4\ln 2 \frac{(\lambda_{BS}-\lambda_{BR})^2}{\Delta\lambda_{BS}^2 + \Delta\lambda_{BR}^2} \right] \right\}. \tag{8}$$

For simplicity, it is assumed that both FBG's have the same spectral width, i.e., $\Delta\lambda_{BS} = \Delta\lambda_{BR} = \Delta\lambda_B$. Therefore, also considering relation (1), the output power from the system under study is

$$P_D = \frac{k^2(1-k)^2}{\sqrt{2}} P_0 R_{0S} R_{0R} \frac{\Delta\lambda_B}{\Delta\lambda_0} \beta(\lambda_{BS})\alpha(\lambda_{BS}), \tag{9}$$

with

$$\beta(\lambda_{BS}) = \exp\left[-4\ln 2 \left(\frac{\lambda_{BS}-\lambda_0}{\Delta\lambda_0} \right)^2 \right], \tag{10}$$

$$\alpha(\lambda_{BS}) = \exp\left[-2\ln 2 \left(\frac{\lambda_{BS}-\lambda_{BR}}{\Delta\lambda_B} \right)^2 \right], \tag{11}$$

where P_0 is the total power injected into the fiber by the optical source.

When the FBG_R scans in wavelength the light reflected by the FBG_S, the optical power at the output of the system (P_D) will change following an exponential relation given by Eq. (11). Term $\alpha(\lambda_{BS})$ corresponds to the overlap area of the two FBG's spectral distributions for a particular value of the difference $\lambda_{BS} - \lambda_{BR}$. So, in fact, it represents the normalized convolution function between the two Gaussian functions, $G_S(\lambda)$ and $G_R(\lambda)$. To compare the utilization of the Gaussian reflectivity function [Eq. (5)] and the real reflectivity function [Eq. (2)], we calculated the numerical autoconvolution of $R(\lambda)$. Figure 3 shows the autoconvolution functions obtained from the reflectivity profiles illustrated in Fig. 2. They are clearly similar, especially when the behavior far from the central wavelength is neglected. This result is a consequence of the smoothing properties of the convolution operation. Therefore, in the context of the problem being analyzed, it is reasonable to use the Gaussian approximation for the fiber Bragg grating reflectivity profile.

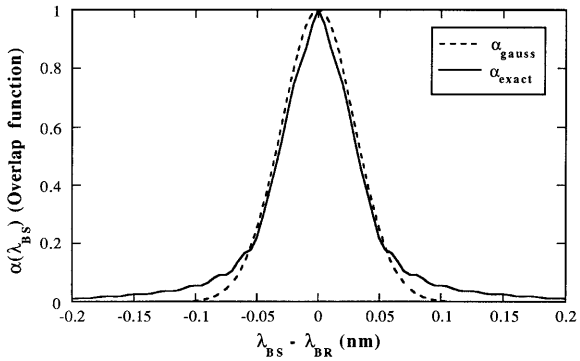

Fig. 3. Normalized autoconvolution functions obtained from the FBG spectral reflectivity profiles, considering the exact model (α_{exact}) and the Gaussian approximation (α_{gauss}).

3. Sensitivity Analysis

In this section, and considering the primary noise sources (shot noise and electronic noise), the minimum Bragg wavelength shift in the sensing grating detected by the system is evaluated.

A variation of $\delta\lambda_{BS}$ in the Bragg wavelength of the FBG sensor will produce a variation in the optical power arriving at the detector (δP_D) such that

$$\delta\lambda_{BS} = \frac{1}{(\mathrm{d}P_D/\mathrm{d}\lambda_{BS})}\,\delta P_D, \tag{12}$$

where $\mathrm{d}P_D/\mathrm{d}\lambda_{BS}$ is the derivative of Eq. (9) with relation to λ_{BS} and is given by

$$\frac{\mathrm{d}P_D}{\mathrm{d}\lambda_{BS}} = \left(\frac{k^2(1-k)^2 P_0 R_{0S} R_{0R} \Delta\lambda_B}{\sqrt{2}\Delta\lambda_0} \right) \frac{\mathrm{d}}{\mathrm{d}\lambda_{BS}}(\beta\alpha). \tag{13}$$

When $\Delta\lambda_0 \gg \Delta\lambda_B$ and $(\mathrm{d}\alpha/\mathrm{d}\lambda_{BS}) \gg (\mathrm{d}\beta/\mathrm{d}\lambda_{BS})$, which is normally the case, it follows that

$$\frac{\mathrm{d}P_D}{\mathrm{d}\lambda_{BS}} \approx A\beta \frac{\mathrm{d}\alpha}{\mathrm{d}\lambda_{BS}}, \tag{14}$$

with

$$A = P_0 \frac{k^2(1-k)^2 R_{0S} R_{0R}}{\sqrt{2}} \frac{\Delta\lambda_B}{\Delta\lambda_0}. \quad (15)$$

Hence, for a signal-to-noise ratio of one, the minimum detectable Bragg wavelength shift in the presence of a particular noise source (j) is

$$\delta\lambda_{BS}\big|_j = \frac{1}{[A\beta(d\alpha/d\lambda_{BS})]} \sqrt{BH_j}, \quad (16)$$

where, for that particular noise source, H_j is the equivalent one-sided spectral density of the squared equivalent optical noise and B is the detection bandwidth.[15] Assuming that all the noise sources are uncorrelated, the minimum detectable Bragg wavelength shift is

$$\delta\lambda_{BS}|_{\min} = \left[\sum_j (\delta\lambda_{BS}|_j)^2\right]^{1/2}. \quad (17)$$

The shot-noise current generated in the detection process (rms value) is given by

$$i_{\text{shot}} = (2eM^2F\Re BP_D)^{1/2}, \quad (18)$$

where e is the electron charge, F is the detector excess noise factor, M is the photodetection gain ($M = 1$ if a p-i-n photodiode is used), and $\Re$ is the detector responsivity, which is given by $\Re = \eta e/h\nu$, with η being the detector quantum efficiency, h the Planck constant, and ν the optical frequency of the radiation. Considering that the current generated in the detector is proportional to the incident optical power (P_D), it is convenient to express the shot-noise current in terms of an equivalent optical noise, with H_{shot} given by

$$H_{\text{shot}} = \frac{{i_{\text{shot}}}^2}{B\Re^2} = \frac{2M^2Fh\nu P_D}{\eta}. \quad (19)$$

Combining the previous relations, one obtains the normalized minimum detectable Bragg wavelength shift that is due to shot noise:

$$\left.\frac{\delta\lambda_{BS}}{\sqrt{B}}\right|_{\text{shot}} = \frac{{\Delta\lambda_B}^2}{4\ln 2(\lambda_{BR} - \lambda_{BS})\sqrt{A\beta\alpha}} \left(\frac{M^2Fh\nu}{\eta}\right)^{1/2}, \quad (20)$$

where β and α are given by Eqs. (10) and (11), respectively.

Other noise sources must be considered, namely the shot noise associated with the dark current of the detector (i_{dark}), the thermal noise generated in the feedback resistance of the transimpedance amplifier (R_f), and the noise generated in the amplifier itself (i_{amp}). Lumping these noise sources together as electronic noise, we find that the correspondent $H_{\text{electronic}}$ is given by[15]

$$H_{\text{electronic}} = \left(\frac{h\nu}{\eta e}\right)^2 \left(2eM^2Fi_{\text{dark}} + \frac{4k_BT}{R_f} + {i_{\text{amp}}}^2\right). \quad (21)$$

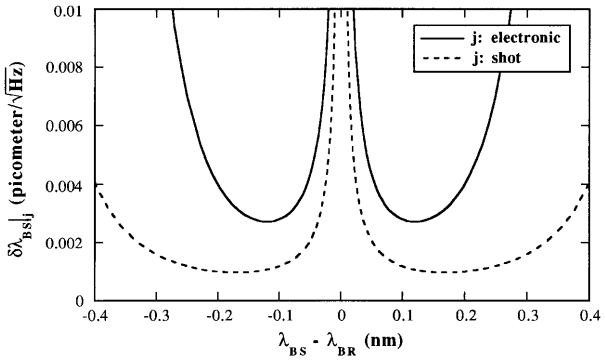

Fig. 4. Minimum detectable Bragg wavelength shift as determined by shot and electronic noise, assuming perfect Gaussians for $G_S(\lambda)$ and $G_R(\lambda)$ and identical linewidths.

Again combining the previous relations, we find that the normalized minimum detectable Bragg wavelength shift that is due to electronic noise is expressed as

$$\left.\frac{\delta\lambda_{BS}}{\sqrt{B}}\right|_{\text{electronic}} = \frac{{\Delta\lambda_B}^2 h\nu}{4\ln 2(\lambda_{BS} - \lambda_{BR})A\beta\alpha\eta e} \times \left(2eM^2Fi_{\text{dark}} + \frac{4k_BT}{R_f} + {i_{\text{amp}}}^2\right)^{1/2}. \quad (22)$$

Figure 4 shows the normalized minimum detectable Bragg wavelength shift, assuming perfect Gaussians with equal linewidths, determined by electronic and shot noise, as predicted by Eqs. (20) and (22) and using the following values: $L = 10$ mm; $\Delta n = 1.0 \times 10^{-4}$ (typical value); $n_{\text{eff}} = 1.453$; $\chi = 0.7$; $\Delta\lambda_{BS} = \Delta\lambda_{BR} = 0.2$ nm; $R_{0S} = R_{0S} = 80\%$; $k = 0.5$; $\Delta\lambda_0 = 70$ nm; $P_0 = 0.1$ mW; $\lambda_{BS} = \lambda_{BR} = 835$ nm; $\lambda_0 = 830$ nm; $M = F = 1$ (for a p-i-n diode); $\Re = 0.85$ A/W ($\eta = 0.68$); $i_{\text{dark}} = 1.3$ nA; $R_f = 2$ MΩ; $i_{\text{amp}} = 0.01$ pA/$\sqrt{\text{Hz}}$ (for the electronic OP15 OpAmp); and $T = 300$ K. As expected, the best resolution occurs when the receiving grating is detuned from the sensing grating by a certain amount, $\Delta\lambda = \lambda_{BS} - \lambda_{BR} = \Delta\lambda_{\text{opt}}$. This value is noise source dependent; however, its specification is more critical in the numerical example analyzed when electronic noise is considered. In this case $\Delta\lambda = 0.12$ nm, resulting in $(\delta\lambda_{BS}/\sqrt{B})|_{\text{electronic}} \approx 2.7 \times 10^{-3}$ pm/$\sqrt{\text{Hz}}$.

Taking into account the intrinsic sensitivities to temperature and strain of fiber Bragg gratings (typical values of 5.86 pm/°C and 0.65 pm/μstrain, respectively), we find that the system sensitivity to these parameters is 4.6×10^{-4} °C/$\sqrt{\text{Hz}}$ and 4.2×10^{-3} μstrain/$\sqrt{\text{Hz}}$, respectively. Figure 4 clearly indicates that for the present example, electronic noise is dominant relatively to shot noise. Therefore, the system sensitivity could be improved by, for example, utilizing an avalanche photodiode with appropriate gain and a very low-noise operational amplifier. However, it must be emphasized that when the system is used to measure quasi-static parame-

ters, such as strain and temperature, the sensitivity achievable is substantially degraded compared with the values stated above because of the presence of other noise sources that are difficult to quantify, for example, noise sources with frequency dependence of the type $1/f$.

4. Experiment

The system configuration used to analyze the sensitivity of the matched FBG interrogation scheme is shown in Fig. 1. A pigtailed superluminescent source (Superlum SLD-361/A, $\lambda_0 = 826.7$ nm, $\Delta\lambda_0 = 20.2$ nm, $P_0 = 0.55$ mW) was used to illuminate the system. The reflectivity of the sensing grating (FBG_S) and its spectral characteristics were measured at room temperature and with no axial strain applied to the fiber grating. The results are as follows: reflectivity $\approx$17%, $\lambda_{BS} = 835.4$ nm, and $\Delta\lambda_{BS} \approx 0.2$ nm. For the receiving grating (FBG_R) the measured reflectivity was $\approx$45% and the spectral characteristics were close to those of FBG_S. These values were obtained by using a optical spectrum analyzer (ANDO AQ-6312B; maximum resolution, 0.1 nm). The reflected light from the sensing grating was sent to the receiving grating by means of a 3-dB ($k = 0.5$) coupler. With the use of another 3-dB coupler, light, after being again reflected by this grating, was detected by using a pigtailed hybrid photodetector with integrated amplification (from United Optoelectronics Laboratory Ltd., RM 800/2). The overall effective responsivity was 37 V/μW and the noise equivalent power was 0.46 pW/$\sqrt{\text{Hz}}$ at 1 kHz. When the central reflecting wavelength of the FBG_R is linearly swept over the wavelength working range of the FBG_S by driving the piezoelectric transducer, then at some point in the sweep the two FBG's will start to match, resulting in an increasing signal being backreflected from the FBG_R and detected by the photodiode. This signal will be maximum when the two Bragg wavelengths completely match, i.e., $\lambda_{BS} - \lambda_{BR} = 0$. As a way to measure the sensitivity of the demodulation scheme, a small amplitude strain signal ($3\mu\varepsilon$) with a frequency of 1 kHz was applied to the sensing grating. Then, for each point in the sweep of the receiving grating, the system signal-to-noise ratio was measured by using an electric spectrum analyzer.

5. Results and Discussion

Figure 5(a) shows the measured system output power level when the FBG_S is linearly scanned by the FBG_R, which is proportional to the convolution between the distributions of both gratings. The structure of the experimental convolution curve is quite different from the one shown in Fig. 3. We believe this deviation is due to the particular spectral distribution of each grating, which was far from being perfectly Gaussian. This was confirmed by measuring their spectral characteristics by using a computer-controlled monochromator with a resolution of 10 pm (Jobin-Yvon THR1000). Results of these measurements are shown in Figs. 6(a) and 6(b).

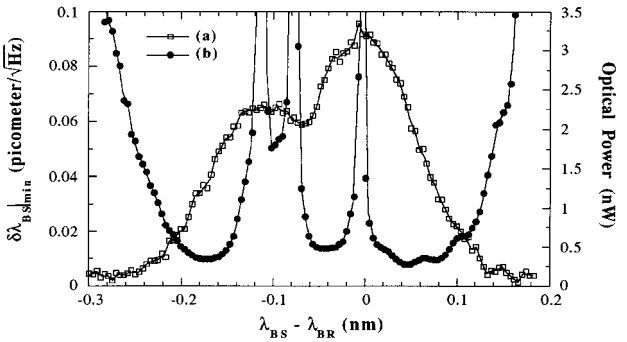

Fig. 5. (a) Measured system output power level. (b) Experimental determined system sensitivity.

The obtained data clearly explain the secondary lobe present in the detected power curve [Fig. 5(a)]. Significant is the fact that the FBG_R has a narrower linewidth than the FBG_S, which has a strongly irregular (non-Gaussian) spectral distribution.

According to relation (12) and considering the form of the experimental optical power curve in Fig. 5(a), four points of maximum sensitivity and three points of minimum sensitivity were expected. This is confirmed by the experimental results shown in Fig. 5(b), where the minimum detectable Bragg wavelength shift is plotted against the Bragg wavelength difference between the two gratings. The experimental results have a sensitivity dependence similar to the theoretical curve shown in Fig. 4, where it was as-

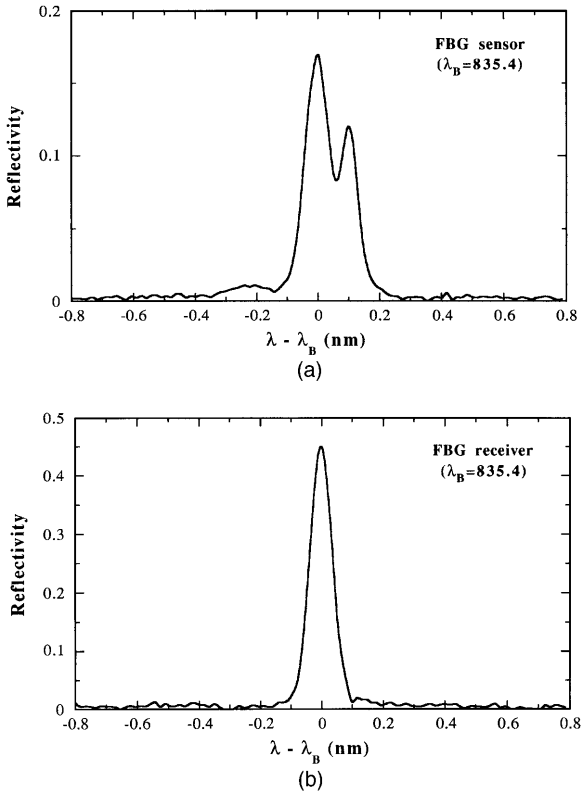

Fig. 6. Spectrum of the fiber Bragg gratings: (a) sensing grating, (b) receiving grating.

sumed that the spectral distributions of the gratings were perfectly Gaussian and with equal linewidths. Obviously, for a perfect Gaussian distribution, only two maximum sensitivity points are expected, as shown in the figure. Substitution of the measured noise equivalent power, and all the parameters in the experiment, into Eqs. (22) and (20) leads to $\delta\lambda_{BS}|_{\text{electronic}} \approx 0.01$ pm/$\sqrt{\text{Hz}}$ and $\delta\lambda_{BS}|_{\text{shot}} \approx 8.3 \times 10^{-4}$ pm/$\sqrt{\text{Hz}}$, respectively. From these values one obtains $\delta\lambda_{BS}|_{\text{min}}$ very near to the one in Fig. 5(b), showing a good agreement between the theoretical model and the experimental results (for $\lambda_{BS} - \lambda_{BR} = +0.08$ nm, the example value used in these calculations). The experimental results also demonstrate that extreme care must be taken during the fabrication process of the receiving and sensing gratings to obtain similar spectral characteristics. In fact, if this is not achieved, the system resolution can be substantially decreased even when the two gratings are slightly mismatched. As an example, the point $\lambda_{BS} - \lambda_{BR} = -0.08$ nm in Fig. 5 corresponds to a high value for the minimum detectable Bragg wavelength shift.

Naturally, the operation of the system at the condition of maximum sensitivity is desirable. This can be achieved by applying a small amplitude sinusoidal signal to the receiving grating, which is locked by a servo loop to the point where the correspondent output signal is at the maximum (for gratings with smooth Gaussian profiles, there are two of these points). If the receiving grating is kept in a controlled environment, the feedback voltage applied to this grating is proportional to the wavelength changes induced in the sensing grating (within the servo bandwidth).

6. Conclusion

It was theoretically shown that there is an optimum Bragg wavelength difference between the receiving and sensing gratings that maximizes the sensitivity when the reflective-matched fiber Bragg grating sensing interrogation scheme is used. Experimental results were obtained that confirm this prediction. In addition, it was shown that a nonregular spectral distribution of the gratings can compromise the sensitivity in this demodulation scheme.

The authors thank J. M. Sousa for all the help given in the computer simulations. A. B. Lobo Ribeiro and L. A. Ferreira acknowledge the financial support from Programa PRAXIS XXI.

References

1. W. W. Morey, G. Meltz and W. H. Glenn, "Fibre optic Bragg grating sensors," in *Fiber Optic and Laser Sensors VII*, R. P. DePaula and E. Udd, eds., Proc. SPIE **1169,** 98–107 (1989).
2. W. W. Morey, "Distributed fiber grating sensors," in *Proceedings of the Seventh Optical Fiber Sensors Conference* (Institute of Radio and Electronic Engineers, Sydney, Australia, 1990), pp. 285–288.
3. S. M. Melle, K. Liu, and R. M. Measures, "A passive wavelength demodulation system for guided-wave Bragg grating sensors," IEEE Photon. Technol. Lett. **4,** 516–518 (1992).
4. A. D. Kersey, T. A. Berkoff, and W. W. Morey, "Multiplexed fiber Bragg grating strainsensor system with a fiber Fabry–Perot wavelength filter," Opt. Lett. **18,** 1370–1371 (1993).
5. M. A. Davis and A. D. Kersey, "All-fibre Bragg grating strainsensor demodulation technique using a wavelength division coupler," Electron. Lett. **30,** 75–77 (1994).
6. Q. Zhang, D. A. Brown, H. Kung, J. E. Townsend, M. Chen, L. J. Reinhart, and T. F. Morse, "Use of highly overcoupled couplers to detect shifts in Bragg wavelength," Electron. Lett. **31,** 480–482 (1995).
7. M. G. Xu, H. Geiger, J. L. Archambault, L. Reekie, and J. P. Dakin, "Novel interrogating system for fibre Bragg grating sensors using an acousto-optic tunable filter," Electron. Lett. **29,** 1510–1511 (1993).
8. A. D. Kersey, T. A. Berkoff, and W. W. Morey, "High-resolution fibre-grating based strain sensor with interferometric wavelength-shift detection," Electron. Lett. **28,** 236–238 (1992).
9. D. A. Jackson, A. B. Lobo Ribeiro, L. Reekie, and J. L. Archambault, "Simple multiplexing scheme for fibre optic grating sensor network," Opt. Lett. **18,** 1192–1194 (1993).
10. G. P. Grady, S. Hope, A. B. Lobo Ribeiro, D. J. Webb, L. Reekie, J. L. Archambault, and D. A. Jackson, "Bragg grating temperature and strain sensors," Opt. Commun. **111,** 51–54 (1994).
11. M. A. Davis and A. D. Kersey, "Matched-filter interrogation technique for fibre Bragg grating arrays," Electron. Lett. **31,** 822–823 (1995).
12. T. A. Berkoff, M. A. Davis, and A. D. Kersey, "Source structure induced measurement errors in fiber Bragg grating sensor arrays," in *Distributed and Multiplexed Fiber Optic Sensors IV*, J. P. Dakin and A. D. Kersey, eds., Proc. SPIE **2294,** 60–68 (1994).
13. S. Huang, M. LeBlanc, M. M. Ohn, and R. M. Measures, "Bragg intragrating structural sensing," Appl. Opt. **34,** 5003–5009 (1995).
14. H. G. Limberger, P. Y. Fonjallaz, and R. P. Salathé, "Spectral characterisation of photoinduced high efficient Bragg gratings in standard telecomunication fibres," Electron. Lett. **29,** 47–49 (1993).
15. J. L. Santos and D. A. Jackson, "Coherence sensing of time-addressed optical-fiber sensors illuminated by a multimode laser diode," Appl. Opt. **30,** 5068–5076 (1991).